Available online at www.sciencedirect.com
ScienceDirect
International Journal of Heat and Mass Transfer 51 (2008) 1409–1422
International Journal of HEAT and MASS TRANSFER
www.elsevier.com/locate/ijhmt

The relative importance of external and internal transport phenomena in three way catalysts

H. Santos [a], M. Costa [b,*]

[a] Mechanical Engineering Department, School of Technology and Management, Polytechnic Institute of Leiria, Morro do Lena – Alto Vieiro Apt. 4163, 2411-901 Leiria, Portugal
[b] Mechanical Engineering Department, Instituto Superior Técnico, Technical University of Lisbon, Avenida Rovisco Pais, 1049-001 Lisbon, Portugal

Received 24 May 2007; received in revised form 17 September 2007
Available online 26 December 2007

Abstract

The conversion efficiency of three way catalyst (TWC) depends on chemical reaction and transport limitations. This paper reports a quantitative analysis of the relative importance of these limiting processes based on experimental data obtained under real world vehicle operating conditions. The main conclusions are as follows: (i) above light-off temperature the mass transport phenomena overlaps the kinetic limitation but pure external mass transfer control is hard to attain in TWC operating under real world automotive conditions, even when both space velocity and operating temperature are very high; (ii) above light-off temperature the automotive TWC operates in a mixed regime with both internal and external mass transfer playing important roles; (iii) the internal mass transfer limitation is more important to control conversion in the TWC than the external mass transfer limitation but the relative importance of the external mass transfer increases as the temperature rises; (iv) the internal mass transfer limitation cannot be disregard in TWC modeling studies and (v) the results show that the current generation of TWC is over designed from an external mass transport viewpoint so that future improvements of these devices can be achieved with porous washcoat with improved transport proprieties.

Keywords: Three way catalyst; Conversion efficiency; External mass transfer; Internal mass transfer; Chemical reaction

1. Introduction

A typical three way catalyst (TWC) consists of a large number of parallel channels, often in a honeycomb arrangement. Small size channels of these devices provide large surface area [1]. The surface of each channel is covered with a 10–150 μm thick porous layer, commonly called as washcoat [2]. The catalytic washcoat in the monolith converters usually consists of partially sintered γ-Al_2O_3. Crystallites of noble metals (typically Pt, Rh and Pd) are dispersed on the γ-Al_2O_3 support as active catalytic components. Other components are added to the washcoat to stabilize the porous structure; they may also act as active catalytic centers (e.g., CeO_2–ZrO_2) [3]. Catalytic reactions take place on the active sites (noble metal crystallites) located on the surface of porous supporting material (γ-Al_2O_3) [4].

In order to comply with future automotive emission legislation, it is necessary to ensure high catalytic efficiencies of the exhaust gas after treatment systems both during cold start and under normal operating conditions (i.e., after light-off, when the catalyst temperature allows for conversion efficiencies above 50%). This need to achieve conversion efficiencies near 100%, under normal operating conditions, is especially true for the so-called *super-ultra-low-emission vehicles*. Under these circumstances, it is decisive to improve the present understanding of all the relevant processes that occur in TWC devices, in particular those associated with the transport phenomena.

In a recent paper [2], we have reported data for ceramic and metallic TWC operating under real world automotive

* Corresponding author. Tel.: +351 218417378; fax: +351 218475545.
E-mail address: mcosta@ist.utl.pt (M. Costa).

0017-9310/$ - see front matter © 2007 Elsevier Ltd. All rights reserved.
doi:10.1016/j.ijheatmasstransfer.2007.11.005

Nomenclature

A	pre-exponential Arrhenius factor (s^{-1})
$\frac{A}{V}$	mass transfer area per unit of catalyst volume (m^{-1})
$Bi_{m,i}$	ratio of convective to diffusive mass transfer
C_i	concentration of chemical specie i (mol m^{-3})
$C_{w,i}$	concentration of chemical specie i at surface of the washcoat (mol m^{-3})
d	hydraulic diameter of monolith cell channel (m)
d_p	mean pore diameter (m)
D_i	combination of bulk and Knudsen diffusion of the chemical specie i ($m^2\ s^{-1}$)
$D_{b,i}$	bulk diffusion of the chemical specie i ($m^2\ s^{-1}$)
$D_{eff,i}$	effective diffusion of the chemical specie i ($m^2\ s^{-1}$)
$D_{eff,ref}$	effective diffusion of the reference specie ($m^2\ s^{-1}$)
$D_{K,i}$	Knudsen diffusion of the chemical specie i ($m^2\ s^{-1}$)
$D_{m,i}$	molecular diffusion of the chemical specie i ($m^2\ s^{-1}$)
E_a	activation energy (J mol^{-1})
L	length of the channel (m)
$k_{m,i}$	mass transfer coefficient from the bulk gas to the washcoat surface (m s^{-1})
$k_{(ov,i)_S}$	overall surface rate constant of the reacting specie i (m s^{-1})
$k_{(ov,i)_V}$	overall rate constant per volume of washcoat for the reacting specie i (s^{-1})
$k_{S,i}$	effective surface rate constant of the reacting specie i (m s^{-1})
$k_{V,i}$	reaction rate constant per volume of washcoat for the reacting specie i (s^{-1})
M_i	molecular weight of the chemical specie i (kg mol^{-1})
M_{ref}	molecular weight of the reference specie (kg mol^{-1})
P_i	transverse Peclet number of the chemical specie i
Pe_i	axial Peclet number of the chemical specie i
R	universal gas constant (J $mol^{-1}\ K^{-1}$)
R_Ω	effective transverse diffusion length (m)
Re	Reynolds number
R_G	global (total) mass transfer resistance
R_L	internal mass transfer resistance
Sc_i	Schmidt number of the chemical specie i
Sh, Sh_i	Sherwood number, Sherwood number of the chemical specie i
SV	space velocity (reciprocal of the residence time) (s^{-1})
T_g	exhaust gas temperature (K)
T_{ref}	reference temperature (K)
T_W	solid wall temperature (K)
t_c	convection (residence) time (s)
$t_{d,i}$	transverse diffusion time of the chemical specie i (s)
$t_{z,i}$	longitudinal diffusion time of the chemical specie i (s)
$t_{R,i}$	wall reaction time of the chemical specie i (s)
v	flow velocity in the longitudinal direction (m s^{-1})
X_i	fractional conversion of the chemical specie i
w	volumetric washcoat loading per catalyst volume
z	axial length (m)

Greek symbols

δ_C	effective washcoat thickness (m)
ε	pore porosity
τ	pore tortuosity factor
$\phi^2_{S,i}$	square of transverse Thiele modulus of the chemical specie i
$\phi_{L,i}$	washcoat Thiele modulus of the chemical specie i
$\eta_{L,i}$	local effectiveness factor of the chemical specie i
$\eta_{G,i}$	global effectiveness factor of the chemical specie i
ν_g	kinematic viscosity of the exhaust gas mixture ($m^2\ s^{-1}$)

conditions above light-off temperature. In common with previous studies (e.g., [5]), our data showed that in addition to the external mass transfer limitation, both kinetic and internal mass transfer limitations also contributes to reduce the TWC performance even at high temperatures. However, a quantitative analysis of the relative importance of the above mentioned limiting processes in TWC, for different operating conditions, still remains an open issue. This has encouraged us to extend our previous study [2] in order to improve the present understanding of the relevant transport and kinetic phenomena that control the TWC operation.

Related studies included those of Tomašić et al. [1] and Tronconi and Beretta [6]. These authors have obtained experimental data for NO_x selective catalytic reduction (SCR) in laboratory monolith reactors. Subsequently, these investigators have analyzed the data in order to quantify the relative importance of the external and internal mass transport limitations. Despite the importance of both contributions, the experiments they have conducted do not reproduce the operation of TWC used in real automotive exhaust gas applications, as the present study does. In this context, it is important to refer the excellent contributions of Pontikakis [7] and Konstantas [8] that provided the community with extensive experimental data for different TWC tested under legislated driving cycle conditions.

In real world operating conditions, TWC operate with laminar flow [9]. Generally, there are two important types

of potential mass transfer limitations that control the TWC conversion efficiencies, namely: external (or inter phase) and internal (or intra phase) [10]. The former accounts for the diffusion of the reactants from the bulk gas phase to the surface of the washcoat – since the flow is laminar, there are always a laminar boundary layer with a concentration gradient. The latter accounts for internal diffusion within the porous washcoat – in this case, most of the surface area of the porous catalyst lies within the washcoat and, thereby, the reactants diffuse to and from the active catalyst sites where the reaction takes place.

Of both transport phenomena here considerate, the internal mass transfer is by far the most complex. In catalytically active washcoats, the internal mass transfer phenomena of the reacting gases have been mainly studied through numerical investigations [4,9–13]. These numerical studies, which had to use models with a significant degree of complexity in order to explicitly consider diffusion in the washcoat, have provided evidence that the concentration gradients that exist within the washcoat may significantly affect the operation of the monolith catalytic converter, especially above light-off temperatures.

Given the numerical complexity required to account for the internal mass transfer phenomena, some authors [14–17] have studied numerically TWC by excluding from their models the diffusion into the washcoat. The magnitude of the internal mass transfer resistance is characterized by a local effectiveness factor, denoted as $\eta_{L,i}$. Authors such as [14–17] have ignored the effect of internal mass transport on the assumption that the washcoat layer is much thinner than the channel radius. Under this condition, they [14–17] have assumed $\eta_{L,i} = 1$. Please note that $\eta_{L,i}$ varies between 0 and 1 and that the smaller their value the greater their influence. Against this background, it is important to carry out quantitative analysis based on the experimental results from TWC in order to clarify the relevance of the internal mass transfer limitation in TWC conversion efficiency for a wide range of operating conditions above the light-off temperature, as it done in the present study.

The present paper aims to provide a quantitative analysis of the relative importance of the external and internal mass transport phenomena in automotive TWC based on experimental data obtained under real world vehicle operating conditions. The analysis is intended to help researchers in model development and validation providing guidelines for future approaches and thereby indicating directions for future improvements of TWC devices.

2. Instrumentation and test procedures

This section describes the experiments performed and the instrumentation used in this study. Conversion efficiency measurements were made under-steady state vehicle operating conditions with TWC operating temperatures ranging from 638 to 1074 K, i.e., above CO, HC and NO_x light-off temperatures. This range of operating temperatures were chosen because the present study concentrates on the transport phenomena and it is well known that above the light-off temperatures the TWC performance is mainly controlled by the mass transfer [9].

The measurements reported here were carried out on a vehicle equipped with a 2.8 l DOHC V6 spark ignition engine that has multipoint fuel injection. Table 1 lists the main characteristics of the engine. The vehicle was tested on a chassis dynamometer (Maha LPS200) under steady-state conditions for a variety of operating conditions in order to measure the TWC conversion efficiencies. In this study, one commercial TWC has been used and Table 2 lists its main characteristics. To perform the experiments, the catalyst was in turn placed in the so-called under-floor position replacing the original TWC installed on the vehicle.

Engine control on-line data were monitored using a Bosch KTS 500 engine diagnostic scanner connected to a diagnostic link, located within the vehicle below the dashboard. The scanner provided the following engine parameters: intake mass air flow (g/s), intake air temperature (°C), coolant temperature (°C), engine speed (rpm), throttle position (%) and spark advance (deg), among others.

Fig. 1 shows a schematic of the vehicle exhaust system and associated instrumentation for the measurements of the gas emission data upstream and downstream of the TWC. Exhaust gas was sampled from the exhaust pipe through stainless steel probes with the aid of the suction pump as shown in Fig. 1. The analytical instrumentation included a magnetic pressure analyzer for O_2 measurements, non dispersive infrared gas analyzers for CO_2 and CO measurements, a flame ionization detector for HC

Table 1
Main engine characteristics

Number of cylinders	6
Displacement (cm^3)	2792
Bore (mm)	81
Stroke (mm)	90.3
Compression ratio	1:10
Injection system	Motronic M 3.8.1
Number of valves	12 (2 per cylinder)

Table 2
Main technical attributes of the catalyst studied

Substrate type	Square cell ceramic
Cell density (cells cm^{-2})	62 (400 cpsi)
Substrate dimensions (mm)	Diameter = 127; $L = 120$
Catalyst volume (dm^3)	1.52
Uncoated geometric surface area ($m^2\ m^{-3}$)	2740
Coated geometric surface area ($m^2\ m^{-3}$)	2526
Uncoated wall thickness (mm)	0.1651 (6.5 mil)
Mean washcoat thickness (mm)	0.025
Open frontal area uncoated (%)	75.7
Open frontal area coated (%)	69.0
Cell hydraulic diameter uncoated (mm)	1.105
Washcoat material	CeO_2–Al_2O_3
Precious metal loading	7 Pd/1 Rh
Total mass of precious metal (g)	1.159

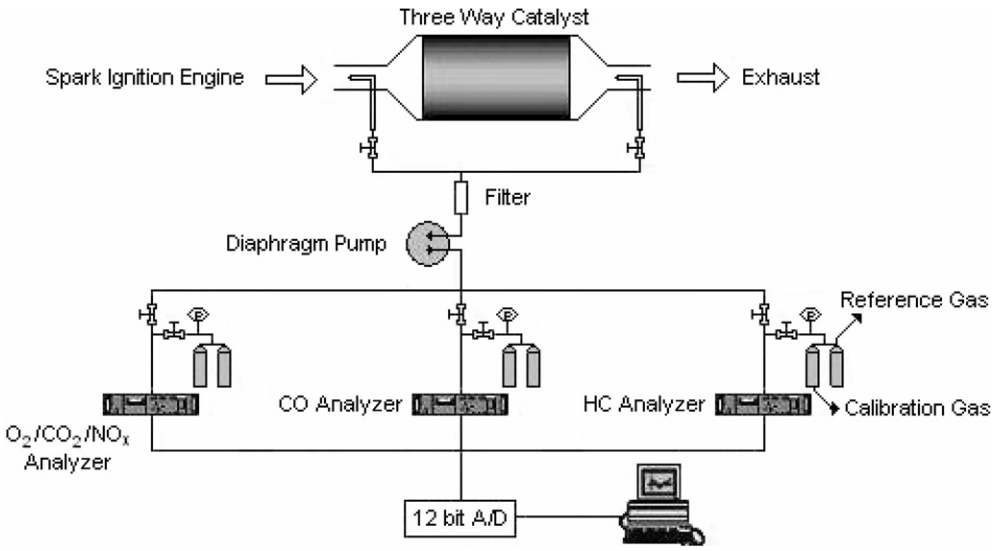

Fig. 1. Schematic of the vehicle exhaust system and associated instrumentation for the measurement of the gas emission data upstream and downstream of the TWC.

measurements and a chemiluminescent analyzer for NO_x measurements. Zero and span calibrations with standard mixtures were performed before and after each measurement session. The maximum drift in the calibration was within ±2% of the full scale.

Fig. 2 shows a schematic of the type K thermocouples location in the vehicle exhaust system for the measurement of the temperatures of the exhaust gases and of the substrate wall. As can be seen in the figure, thermocouples T1 and T6 allowed for the measurement of the exhaust gas temperature (T_g) upstream and downstream of the TWC, and thermocouples T2, T3, T4 and T5 allowed for the measurement of the solid wall temperature. These four thermocouples capture the solid wall temperature gradient

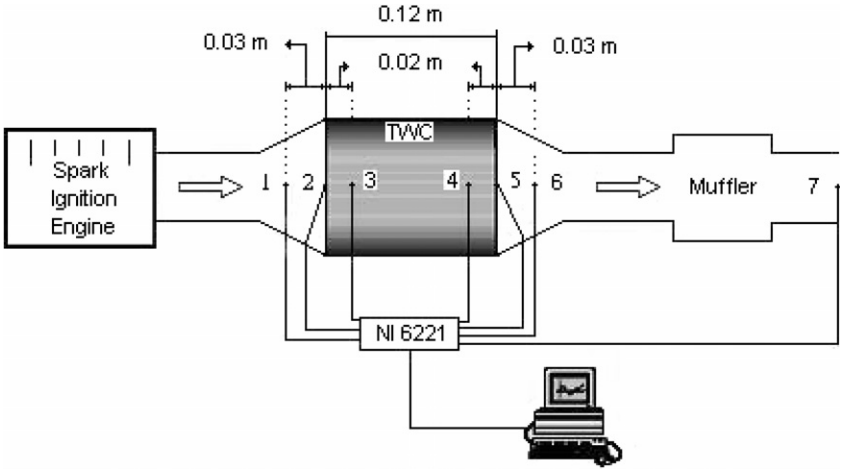

Fig. 2. Schematic of the thermocouples location in the vehicle exhaust system for the measurement of the temperatures of the exhaust gases and of the substrate wall.

Table 3
Test conditions

Vehicle		Ceramic three way catalyst							
Engine speed (rpm)	BMEP (bar)	SV (s^{-1})	Re	P_{HC}	Pe_{HC}	P_{CO}	Pe_{CO}	P_{NO_x}	Pe_{NO_x}
2000	0.00–2.91	18.9–55.4	44.9–91.4	0.032–0.062	6005.3–11777.7	0.018–0.036	3496.5–6855.1	0.016–0.031	3029.7–5939.9
3000	0.00–4.49	34.2–135.2	65.6–155.3	0.045–0.103	8574.9–19498.3	0.026–0.060	4992.6–11352.7	0.023–0.052	4326.0–9837.0
4000	0.00–5.25	53.1–195.2	86.6–199.5	0.059–0.132	11137.5–24904.0	0.034–0.077	6484.7–14500.1	0.030–0.067	5618.9–12564.2

along the monolith reactor length, which depends of the operating conditions. In the present study, the temperature gradient varied between 60 and 100 °C. The solid wall temperature (T_W) used in the present study was taken as the mean value of the four measured temperatures. Finally, thermocouple T7 allowed for the measurement of the temperature of the gases at exit of exhaust manifold.

Table 3 summarizes the test conditions for which the present study was carried out. The engine was tested under steady-state operating conditions (i.e., after engine warm-up). For each engine speed (2000, 3000 and 4000 rpm) tests were made for six different loads (BMEP – break mean effective pressure). In order to establish steady-state operating conditions, the vehicle was operated continuously at a given speed and load for 20–30 min before each measurement session.

3. Dimensionless numbers which characterize flow and reaction

The processes occurring in exhaust after treatment systems for automotive applications involve fluid mechanics, heat and mass transfer and catalytic reactions. To characterize the flow and the reactions the following four characteristic times are used:

$$t_c = \frac{L}{v} \tag{1a}$$

$$t_{d,i} = \frac{(R_\Omega)^2}{D_{m,i}} \tag{1b}$$

$$t_{z,i} = \frac{L^2}{D_{m,i}} \tag{1c}$$

$$t_{R,i} = \frac{(R_\Omega/4)}{k_{S,i}} \tag{1d}$$

The above characteristic times lead to the following three independent dimensionless groups:

$$P_i = \frac{t_{d,i}}{t_c} = \frac{R_\Omega^2 v}{D_{m,i} L} \tag{2a}$$

$$Pe_i = \frac{t_{z,i}}{t_c} = \frac{vL}{D_{m,i}} \tag{2b}$$

$$\phi_{S,i}^2 = \frac{t_{d,i}}{t_{R,i}} = \frac{4R_\Omega k_{S,i}}{D_{m,i}} \tag{2c}$$

where the transverse Peclet number (P_i) represents the ratio of transverse diffusion time to convection time, the axial Peclet number (Pe_i) represents the ratio of axial diffusion time to convection time and the square of transverse Thiele modulus ($\phi_{S,i}^2$) – also referred as the local Damköhler number – represents the ratio of transverse diffusion time to the wall reaction time.

In addition, the definitions of three classical dimensionless groups used in this work are as follows:

$$Re = \frac{vd}{\nu_g} \tag{3a}$$

$$Sc_i = \frac{\nu_g}{D_{m,i}} \tag{3b}$$

$$Sh_i = \frac{k_{m,i} d}{D_{m,i}} \tag{3c}$$

The diffusion coefficients of the HC, CO and NO_x in the exhaust gas mixture have to be calculated. To carry out the calculations of the diffusion coefficients in the gas phase the procedure described in McCullough et al. [18] has been used.

4. The one-dimensional model

Fig. 3 describes schematically the seven main steps involved in the conversion of the exhaust gas pollutants

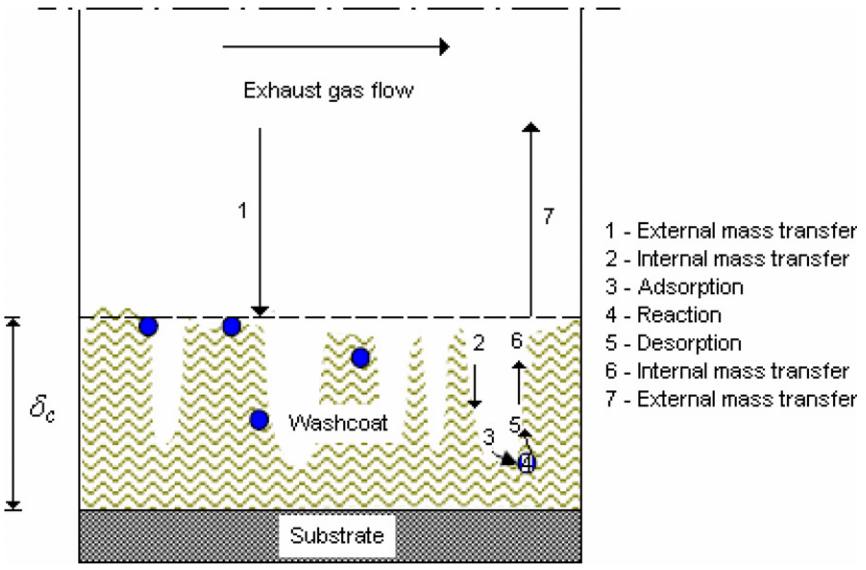

Fig. 3. Schematic representation of the seven main steps involved in the conversion of the exhaust gas pollutants in a channel of a TWC.

in a channel of a TWC, including mass transfer between the bulk gas and washcoat surface, pore diffusion, adsorption/desorption and chemical reaction. In brief, step 1 represents the transport of reactants from the bulk gas to the gas–solid interface (external mass transfer); step 2 represents the internal transport of reactants into the porous washcoat (internal mass transfer); step 3 represents the adsorption of reactants at the interior of catalyst particle; step 4 represents the chemical reaction of adsorbed reactants to adsorbed products; step 5 represents the desorption of adsorbed products; step 6 represents the transport of products from the interior sites to the interface gas–solid of the washcoat and, finally, step 7 represents the transport of products from the gas–solid interface to the bulk fluid stream.

Most of the modeling studies available in the literature for TWC use the "film model" approach (e.g., [14–17]), that approximates the washcoat with a solid–gas interface (zero washcoat thickness), where it is assumed that all reactions occur. This 1D two-phase model essentially neglects the internal mass transfer effects, and assumes that all catalytically active sites are directly available to the gaseous-phase species at this solid–gas interface. For this model, the mass balance for the gas phase is expressed as

$$v\frac{\partial C_i}{\partial z} = -k_{m,i}\frac{A}{V}(C_i - C_{w,i}) \tag{4}$$

The two phases (gas and solid, see Fig. 3) considered by the model are coupled using the transport coefficient for convective mass transfer $k_{m,i}$. External mass transport rates are evaluated through Eq. (3c), and depend of the flow hydrodynamics within the channel and its geometrical proprieties. Modeling studies (e.g., [9]) show that after monolith light-off the reaction is very fast and, consequently, the wall concentration of the reacting species is close to zero along the channel surface. Thus, for this case, the asymptotic Sherwood can be approximated by the value corresponding to the constant wall temperature. The dependence of the asymptotic Sherwood number on the geometrical proprieties of the channel is well documented in the literature [19,20].

In modeling exercises, a commonly simplifying assumption is to model implicitly the pore diffusion and surface reactions, that is, the pore diffusion and the surface reactions are bulked into one overall rate step that includes steps 2–6. This approximation, for the solid–gas interface, states that all gas species that diffuse to it through the boundary layer are removed from the gas phase due to catalytic reactions. In this case, with a first order reaction, the mass balance for the solid phase can be written as

$$k_{m,i}(C_i - C_{w,i}) = k_{S,i}C_{w,i} \tag{5}$$

Rearranging Eq. (5) yields [6]:

$$\frac{1}{k_{(\mathrm{ov},i)_S}} = \frac{1}{k_{m,i}} + \frac{1}{k_{S,i}} \tag{6}$$

where $k_{(\mathrm{ov},i)_S}$ is the overall surface rate constant (measured rate constant). Eq. (6) reflects the resistances to external mass transfer and to catalytic reaction. The reaction rate term, $k_{S,i}$, also known as the apparent rate constant, includes the effects of pore diffusion resistance (internal mass transfer), the amount of catalyst sites (catalyst loading), washcoat properties and the intrinsic reaction adsorption/desorption and reaction rate. With this approach, the washcoat is treated as a black-box without knowledge of the characteristics and details of the phenomena taking place there [16].

The rate of reaction for an automotive TWC can be written in Arrhenius type form with an apparent pre-exponential factor and an apparent activation energy. These factors are tuned in most of the reported models to fit the behavior of the catalyst modeled [15,16]. All of the unknown characteristics are lumped into these parameters. In these models, the internal mass transfer effects and the adsorption–reaction–desorption process is lumped into the tunable parameters [21].

Although the washcoat is a relatively thin coating on the substrate, under certain conditions, the catalytically actives sites on the bottom of the layer may not be as effectively utilized as those on the top of the washcoat layer. Nowadays, internal mass transfer phenomena are receiving increased attention from investigators [4]. In the present study, it has been included in the model explicitly the internal mass transfer phenomena using the local effectiveness factor approach. Accordingly, $k_{S,i}$ is related with $k_{V,i}$ through the following equation:

$$k_{S,i} = \eta_{L,i}\delta_C k_{V,i} \tag{7}$$

In Eq. (7) $k_{V,i}$ accounts only for steps 3–5 (see Fig. 3) and $\eta_{L,i}$ accounts for the internal mass transport within the washcoat (steps 2 and 6 – see Fig. 3). Due to the importance of evaluating accurately $\eta_{L,i}$, Appendix A presents the method that has been used here for its evaluation.

Multiplying Eq. (5) by $\frac{A}{V}$ and using Eq. (7), the solid phase mass balance can be written as

$$k_{m,i}\frac{A}{V}(C_i - C_{w,i}) = \eta_{L,i}wk_{V,i}C_{w,i} \tag{8}$$

Rearranging Eq. (8) yields:

$$\frac{1}{k_{(\mathrm{ov},i)_V}} = \frac{1}{k_{m,i}\frac{A}{V}} + \frac{1}{\eta_{L,i}wk_{V,i}} \tag{9}$$

Note that $k_{(\mathrm{ov},i)_V}$ is related with $k_{(\mathrm{ov},i)_S}$ through the following equation:

$$k_{(\mathrm{ov},i)_V} = k_{(\mathrm{ov},i)_S}\frac{A}{V} \tag{10}$$

The presence of catalytic reactions at the wall of the channel acts as a source or a sink and imposes concentration gradients in the transverse directions. The extent of the transverse variations depends mainly on the relative rate of the mass transfer across the channel, compared to that of the catalytic reactions. At low operating temperatures,

slow reaction rates lead to a nearly uniform concentration distribution within the washcoat. In the literature, this regime is called kinetically controlled [9]. On the other hand, at high temperatures, a sharper increase of the reaction rates, following the Arrhenius law, overlaps the mass transfer process and the TWC operation is reversed to the mass transfer controlled regime [9].

Using Eq. (7), Eq. (5) can be written as follows:

$$\frac{C_{w,i}}{C_i} = \frac{1}{1 + \frac{\eta_{L,i}\delta_C k_{V,i}}{k_{m,i}}} \tag{11}$$

Taking into account the definitions of $\phi^2_{S,i}$ (Eq. (2c)) and Sh_i (Eq. (3c)), results:

$$\frac{\eta_{L,i}\delta_C k_{V,i}}{k_{m,i}} = \frac{\phi^2_{S,i}}{Sh_i} \tag{12a}$$

or

$$\frac{k_{S,i}}{k_{m,i}} = \frac{\phi^2_{S,i}}{Sh_i} \tag{12b}$$

The relative magnitude of $\phi^2_{S,i}$ and Sh_i in Eq. (12a) are indicative of the resistances offered by kinetics plus internal mass transfer, and external mass transfer, respectively. In Eq. (11) two limiting situations can be identified:

- $\frac{C_{w,i}}{C_i} \to 1$ when $\frac{\phi^2_{S,i}}{Sh_i} \to 0$; for this condition, the reaction kinetics are very low and so the process is kinetic controlled.
- $\frac{C_{w,i}}{C_i} \to 0$ when $\frac{\phi^2_{S,i}}{Sh_i} \to \infty$; for this condition, the reaction kinetics are very fast and so the process is external mass transfer controlled.

As a practical criterion, Balakotaiah and West [22] have suggested:

$$\frac{\phi^2_{S,i}}{Sh_i} \leqslant 0.1 \tag{13}$$

for kinetic control, and

$$\frac{\phi^2_{S,i}}{Sh_i} \geqslant 10 \tag{14}$$

for external mass transfer control. Balakotaiah and West [22] have also suggested that both resistances are significant when

$$0.1 \leqslant \frac{\phi^2_{S,i}}{Sh_i} \leqslant 10 \tag{15}$$

5. Results and discussion

5.1. External mass transfer limitations

Table 3 summarizes the tests conditions used in the present study. The laminar flow ($Re < 200$, for the present study) within the small channels of the TWC is less favorable than turbulent flow for external mass transfer, so it is expectable that the diffusive transport of the reactants in TWC from the bulk gas phase to the washcoat surface may be hindered to some extent. The external mass transfer limitation can be analyzed through the evaluation of the observed rate constant, $k_{(\mathrm{ov},i)_V}$. This rate constant is calculated based on experimental measurements through the following expression:

$$k_{(\mathrm{ov},i)_V} = -\mathrm{SV}\ln(1 - X_i) \tag{16}$$

The constant $k_{(\mathrm{ov},i)_V}$ incorporates a combination of chemical kinetics and mass transfer limitations (see Eq. (9)). From Eq. (16) it can be concluded that $k_{(\mathrm{ov},i)_V}$ depends on the hydrodynamic conditions (SV) and on the conversion data (X_i), both measured in the present study. For the present experimental set of measurements, X_i ranged from 91.8% to 97.2%; 76.8% to 90.9% and 96.8% to 99.0%, for CO, HC and NO_x, respectively, and SV ranged from 18.9 to 195.2 s^{-1} (see Table 3).

Based on the measured data, $k_{(\mathrm{ov},i)_V}$ was evaluated using Eq. (16) for each operating condition for the three chemical species under study. Fig. 4 shows an Arrhenius plot of the overall rate constant $k_{(\mathrm{ov},i)_V}$ for CO, HC and NO_x and the limit for pure external mass transfer control. Fig. 4 reveals identical slopes for the three chemical gas species studied. The estimated values for the apparent activation energy calculated through fittings of the experimental data are 27.93, 24.58 and 29.56 kJ mol^{-1} for CO, HC and NO_x, respectively. These values are much lower than those expected for a catalytic reaction with rate controlled only by chemical kinetics. Based on experimental measurements for a commercial TWC, Kwon et al. [23] reported activation energies of 79.0, 92.8 and 63.0 kJ mol^{-1} for CO, HC and NO_x, respectively. As mentioned earlier, the present data were gathered for TWC temperatures (638–1074 K) above light-off so that the observed slopes in Fig. 4 are strongly influenced by mass transfer limitations.

The related study carried out by Tronconi and Beretta [6] reported experimental results for SCR of NO_x also above light-off temperature (571–666 K). These authors have verified that the NO_x slope provides an estimation for the apparent activation energy close to about 16 kJ mol^{-1}. Tomašić et al. [1] have also reported results in the temperature range of 573–773 K and found a value of 28.88 kJ mol^{-1} for the apparent activation energy.

In common with [1,6], the present study demonstrates that also for TWC operation, above light-off, the measured slopes are lower that the kinetic slopes. Tomašić et al. [1] and Tronconi and Beretta [6] have concluded that the mass transport phenomena play an important role in the overall SCR reactor performance above light-off. The present study confirms that this is also the case for TWC operating under real world applications.

The analysis of Tomašić et al. [1] and Tronconi and Beretta [6] are both based on steady-state results, as in the present study. In contrast, Pontikakis [7] and Konstantas [8] obtained their data for TWC with the vehicle

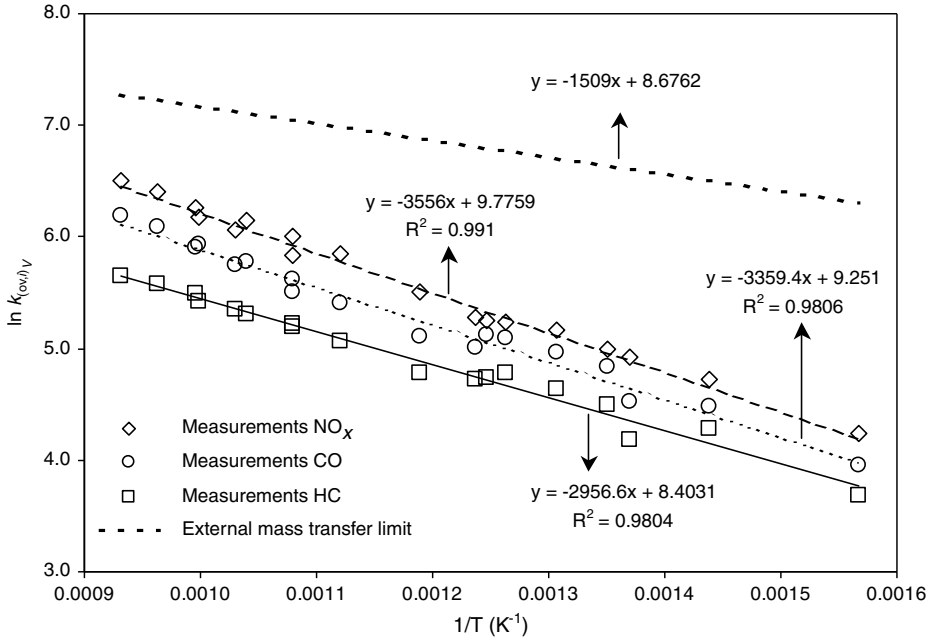

Fig. 4. Arrhenius plot of the overall rate constant $k_{(ov,i)_V}$ for CO, HC and NO_x and the limit for pure external mass transfer control.

operating under standard test conditions which are inherently transient. Konstantas [8] recognized the importance of the determination of the catalysis limiting step between the reaction rate and bulk diffusion (external mass transfer) in the optimization of catalytic converter design. From his transient data, Konstantas [8] defined two resistances, one for diffusion from bulk gas to the solid (external mass transfer) and one for reaction in the solid phase (which includes the internal mass transfer and the catalytic reaction). The obtained results showed that only for TWC operating conditions with high mass flow rates and temperatures the conversion is mainly external mass transfer controlled. When the TWC operating condition is reversed for low mass flow rates and temperatures the conversion is controlled by the transport and reaction phenomena that take place within the washcoat.

Returning to Fig. 4, it is seen that for conversion efficiencies controlled solely by external mass transfer the slope in the Arrhenius diagram is very flat, corresponding to 12.6 kJ mol^{-1}, being much lower than the three measured slopes. Favorable conditions for operating in the external mass transfer controlled regime include high temperatures, short residences times (that is, large SV), and an extremely active catalyst with no internal mass transfer limitations. The measured slopes in the present study indicate that the combined effects of internal mass transfer and multiple reactions within the catalytic washcoat layer cannot be excluded, and also play an important role in the operation of an automobile TWC, even in the case of high temperatures and large SV operating conditions.

The evaluation of the external mass transfer limit (dashed line in Fig. 4) is determined by the asymptotic Sherwood. For the evaluation of external mass transfer coefficients, $k_{m,i}$, for 1D models of laminar flow TWC, both experimental [2,5] and theoretical [19] approaches have been proposed in the literature.

In our previous study [2], the Sherwood number was evaluated based on the conversion efficiency data, with the assumption that $k_{m,i} \approx k_{(ov,i)_S}$. The experimental method used in [2] attains asymptotic Sherwood values (external mass transfer limit) solely when both kinetic and internal mass transfer limitations are not rate limiting. However, in common with other authors [5], our data [2] showed that the calculated *Sh* are always below the asymptotic *Sh* so that experimental correlations derived for each chemical specie in [2] lumps internal mass transfer and kinetic effects.

Both experimental and theoretical correlations can be encountered in 1D TWC models. Chang and Hoang [14] and Koltsakis et al. [15] have adopted experimental and theoretical correlations, respectively. The use of experimental correlation lumps the internal mass transfer limitation in the *Sh* whereas the use of theoretical correlation (asymptotic *Sh*) lumps the internal mass transfer limitation in the kinetic rate expression. Both approaches treat the washcoat as a black-box, and do not account explicitly for the internal mass transfer limitations. The following section quantifies the internal mass transfer limitation in TWC operation in order to account for its relevance when compared with external mass transfer and kinetic limitations.

5.2. Internal mass transfer limitations

Because the active catalyst sites are distributed throughout the washcoat this lead to internal mass transfer resistances and lowers the observed reaction rate $k_{(ov,i)_V}$. In the context of the internal mass transfer within the washcoat, this work concentrates only on the CO oxidation

because the analysis presented below for CO is similar for both the HC oxidation and NO_x reduction.

Fig. 5 shows the measured values of $k_{(ov,CO)_V}$ *versus* the operating temperature in the TWC. Rearranging Eq. (9), to account for external mass transfer and both chemical kinetics and internal mass transfer regimes, the overall rate constant can be modeled through the following equation:

$$k_{(ov,i)_V} = \frac{1}{\frac{1}{k_{m,i}\frac{A}{V}} + \frac{1}{\eta_{L,i} w k_{V,i}}} \tag{17}$$

where the first term in the denominator represents the external mass transfer limitation, and the second term represents the internal mass transfer plus the chemical kinetics limitations. As discussed in the previous section, the external mass transport coefficient, $k_{m,i}$, was evaluated through Eq. (3c) with the asymptotic *Sh*. The internal mass transport was evaluated explicitly from $\eta_{L,i}$ (see Eq. (A.2)). The accurate knowledge of the $D_{\text{eff},i}$ is crucial for the evaluation of $\eta_{L,i}$. Appendix B presents the method used to carry out the calculations of $D_{\text{eff},i}$ in the porous washcoat. The rate constant, $k_{V,i}$, was modeled through the Arrhenius rate expression:

$$k_{V,i} = A\, e^{\left(-\frac{E_a}{RT_W}\right)} \tag{18}$$

Eqs. (17) and (18) were fitted to the experimental data in Fig. 5 yielding $A = 2.06 \times 10^8\ s^{-1}$ and $E_a = 59.6\ kJ\ mol^{-1}$. This value for the CO activation energy is lower to the one reported in the literature, which is 79.0 kJ mol^{-1} [23]. The reason for the lower value of E_a found in the present work is because the present experiments have been carried out above the light-off temperature, whereas the activation energy reported by Kwon et al. [23] was obtained from the so-called light-off curve. However, there are sufficient evidence in the literature that above light-off temperature the activation energy attains lower values [12], as observed in the present study.

Fig. 5 clearly shows that even at TWC high temperature operation the strong kinetic limitation is due to the fact that this includes also the internal mass transport limitation. Fig. 5 also reveals that pure external mass transfer control may be hard to attain in automotive TWC.

Fig. 6 identifies the controlling regimes, as typified by Eq. (12b), as a function of the operating temperature in the TWC. The figure shows that $\frac{\phi^2_{S,CO}}{Sh_{CO}}$ is not high enough to achieve a pure external mass transfer controlled regime. This indicates that the characteristic reaction time given by Eq. (1d) is of the same order of magnitude of the transverse diffusion time given by Eq. (1b). Fig. 6 reveals that the values calculated through Eq. (12b) vary from 0.10 to 0.43 and also that above light-off temperature the automotive TWC operates in a mixed regime. This conclusion is consistent with the observations of Konstantas [8] from his CO conversion data from three different commercial TWC.

Considering $\eta_{L,CO} = 1$ in Eq. (17) enables to separate the kinetic limitation from the internal mass transfer limitation. With no internal mass transfer limitation, the values for $k_{(ov,CO)_V}$ can be evaluated from Eq. (17). To this end, the asymptotic *Sh* has been used to evaluate $k_{m,CO}$ and Eq. (18) to evaluate $k_{V,CO}$.

Fig. 7 shows the predicted values of $k_{(ov,CO)_V}$ *versus* the operating temperature in the TWC with no internal mass transfer limitation. This figure also includes the measured values of $k_{(ov,i)_V}$. Comparing the predicted values of $k_{(ov,CO)_V}$, with no internal mass transfer limitation, with the measured values of $k_{(ov,CO)_V}$, it can be seen that the predicted values are much higher than the measured ones. This reveals the importance of internal mass transfer

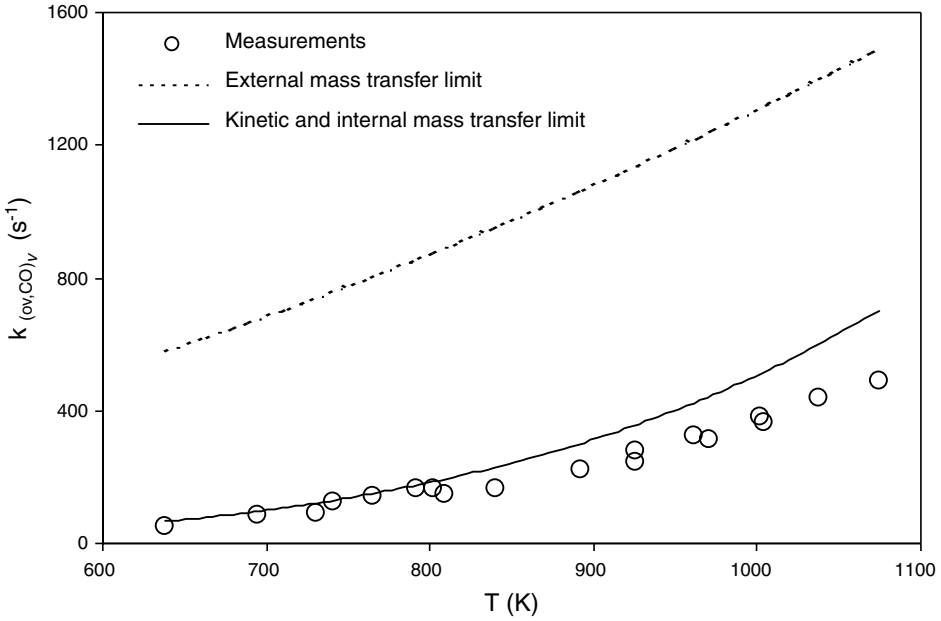

Fig. 5. Measured values of $k_{(ov,i)_V}$ *versus* the operating temperature in the TWC.

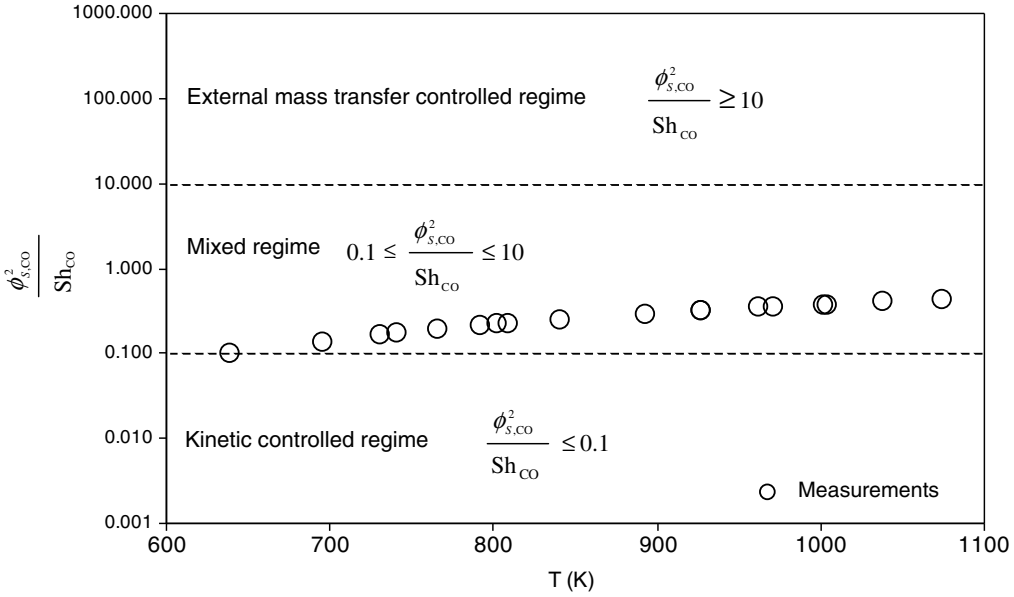

Fig. 6. Controlling regimes, as typified by Eq. (12b), as a function of the operating temperature in the TWC.

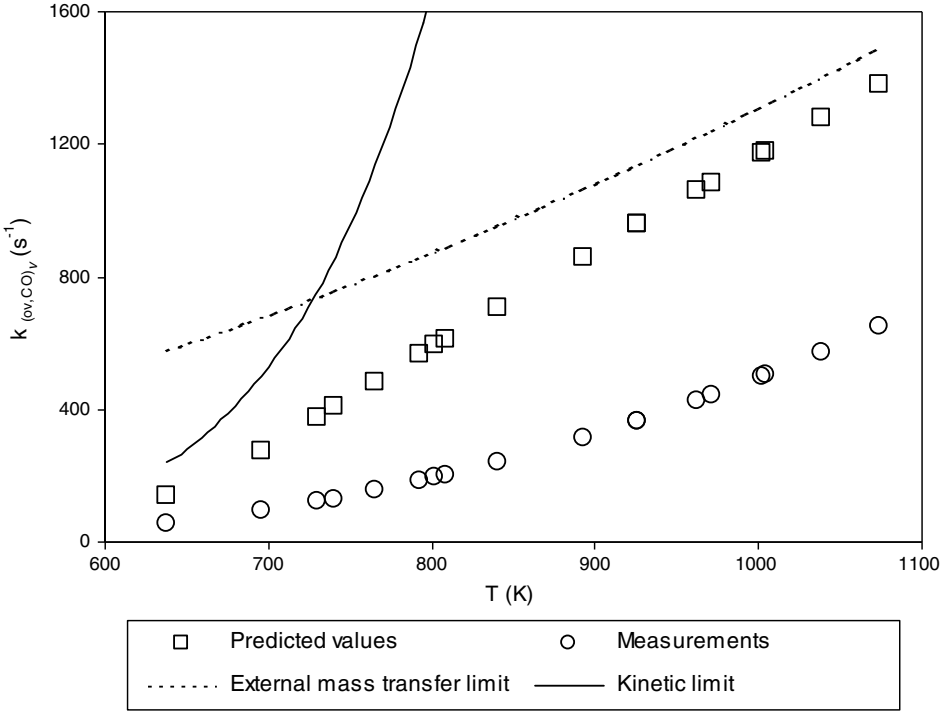

Fig. 7. Predicted values of $k_{(ov,CO)_V}$ *versus* the operating temperature in the TWC with no internal mass transfer limitation.

limitation in the TWC conversion efficiency. The measured values in Fig. 7 reveals that the TWC never attains pure external mass transfer controlled regime for present operating conditions. On the other hand, Fig. 7 shows that if no internal mass transfer limitation exists, the TWC performance is controlled by external mass transfer above temperatures close to about 730 K.

From the discussion above, it can be concluded that if no internal mass transfer limitation exists the TWC conversion efficiency is strongly enhanced. This can be illustrated with the following example: the present experimental data for CO oxidation conversion efficiency range from 91.8% to 97.2%. If no internal mass transfer limitation exists the conversion efficiency would be always above 99.9% for all the experimental conditions.

For the geometrical proprieties of the present TWC and flow conditions studied, the external mass transfer controlled regime imposes an upper limit on the conversion efficiency. However, even when both space velocity and operating temperature are very high it is difficult to operate

under pure external mass transfer controlled conditions, and therefore the current generation of TWC is over designed from an external mass transport point view. The continuous decrease in the tolerable levels of emissions will require a closer examination of the effect of washcoat diffusion on the conversion efficiencies in order to find ways of increasing the washcoat effectiveness for a given precious metal loading. In this context, washcoat layers able to provide higher effectiveness factors, with optimized washcoat pore size distribution, to improve the catalytic active sites utilization are crucial for further improvements of this type of devices.

5.3. Relative importance of external and internal mass transport phenomena

The previous sections discussed the importance of both external and internal transport phenomena in the TWC performance above light-off temperatures. This section quantifies the relative magnitude of the external and internal mass transfer resistances. The global resistance to mass transfer may be expressed as a sum of the external and internal resistances, as shown by Aris [24]. For a first order reaction this may be written as

$$\frac{1}{\eta_{G,i}} = \frac{1}{\eta_{L,i}} + \frac{\phi_{L,i}^2}{Bi_{m,i}} \tag{19}$$

The term that represents the global effectiveness factor, denoted by $\eta_{G,i}$, quantify the combined effects of the external and internal mass transfer limitations. In Eq. (19), the $Bi_{m,i}$ is the mass Biot number defined in terms of the mass transfer coefficient, $k_{m,i}$:

$$Bi_{m,i} = \frac{k_{m,i} \cdot \delta_c}{D_{\text{eff},i}} \tag{20}$$

The Biot number represents a ratio between the convective and the diffusive mass transfer. In the present study, the $Bi_{m,i}$ values ranged from 31.91 to 63.51.

The relative magnitude of the external and internal resistances will depend on the operating parameters of the TWC, namely operating temperature, gas velocity, reactant concentration and physical proprieties.

Fig. 8 presents a comparison between the internal mass transfer resistance (R_L) and the global mass transfer resistance (R_G) at different TWC operating temperatures. The external resistance is simply the difference between the two resistances. The figure shows that the global resistance, due to mass transfer, rises with the temperature. On the other hand, Fig. 8 also shows that the relative importance of the external mass transfer also rises with the temperature. Depending on the value of the TWC operating temperature, both external and internal mass transfer resistances may be significant. However, it is important to note that the internal mass transfer resistance, within the washcoat, controls the conversion efficiency of the TWC in a more extensive way than the external mass transfer resistance.

The data in Fig. 8 also show that for the wide range of temperatures studied above light-off, internal mass transfer effects are significant and cannot be neglected. These results are in good agreement with the numerical results recently reported by Kočí et al. [4] and Hayes et al. [13]. Most researchers on monolith reactors have assumed that the washcoat is so thin that diffusion resistance is not important, and used a local effectiveness factor of unity, e.g., [25]. Doory [25] have investigated the kinetics of the CO

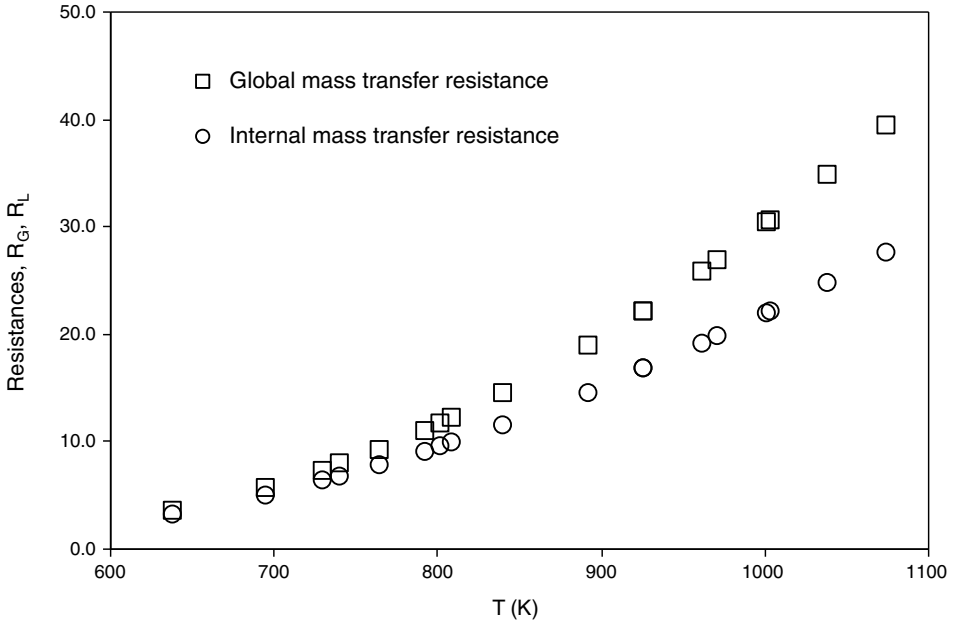

Fig. 8. Comparison of internal mass transfer resistance (R_L) with the global mass transfer resistance (R_G) at different TWC operating temperatures.

oxidation using a monolith reactor operating with the temperature between 556 and 833 K. At higher temperatures the apparent activation energy decreased markedly, as observed in the present study, but Doory attributed this effect to the external mass transfer resistance rather than to the internal mass transfer resistance. The present results show that not recognizing the internal mass transfer limitation can lead to erroneous conclusions regarding the activity of the monolith reactor.

When the mass transfer limitation within the washcoat is significant, the washcoat utilization is poor and thus the reaction takes place mainly next to the interface gas–solid, which is equivalent to a thinner washcoat layer. At the extreme limit (higher temperatures), all reactions take place at the interface and the reactions are only external mass transfer controlled.

From the above discussion, it can be concluded that both external and internal mass transfer limitations have to be considered when modeling TWC for automotive applications. Even for a washcoat layer with 25 μm thickness, the internal mass transport cannot be ignored. This indicates that the consideration of effectiveness factors of unity strong underestimates the internal mass transfer which leads to an overestimation of the TWC performance using 1D two-phase models. When thicker catalytic layers (>25 μm) are used it is expected that the predominance of internal mass transfer limitation increases, as compared with the external mass transfer limitation.

6. Conclusions

As expected, above light-off temperature the mass transport phenomena overlap the kinetic limitation. However, pure external mass transfer control is hard (if not impossible) to attain in TWC operating under real world automotive conditions, even when both the space velocity and the operating temperature are very high.

Above light-off temperature the automotive TWC operates in a mixed regime with both internal and external mass transfer playing important roles. The internal mass transfer limitation is more important to control conversion in the TWC than the external mass transfer limitation. However, the relative importance of the external mass transfer increases as the temperature rises.

The present results demonstrate that the internal mass transfer limitation cannot be disregard in TWC modeling studies.

Finally, the results show that the current generation of TWC is over designed from an external mass transport viewpoint so that future improvements of these devices can be achieved with porous washcoat with improved transport proprieties.

Acknowledgement

The first author (H. Santos) is pleased to acknowledge the Fundação para a Ciência e Tecnologia (FCT) for the provision of a scholarship SFRH/BD/32851/2006. The authors would like to thank technician Manuel Pratas who assisted them in conducting the experimental work presented here.

Appendix A. Evaluation of the local effectiveness factor

The magnitude of the local effectiveness factor, which in general varies from 0 to 1, indicates the relative importance of internal mass transfer resistance. At low effectiveness factor values, most of the reaction takes place near the exposed surface of the washcoat. It should be noted that the local effectiveness factor can exceed the unity in non-isothermal washcoat and for cases of complex chemical kinetics, such as LH (Langmuir–Hinshelwood) type rate expressions [26]. LH type rate expressions are available in the literature for automotive TWC [21,27]. In the case of the automotive TWC washcoats, there are many different species diffusing simultaneously in the washcoat and participating in more than one reaction. Moreover, LH rate expressions are not exactly of the first order because of the inhibition term.

For the present range of operating temperatures and with the concentrations present in the exhaust, the inhibition term of the LH type rate expressions was evaluated and verified to be marginal. For this reason, the additional detail of LH rate expressions were not considered here, since they become important only under low temperature operation such as cold start operation [27]. Additionally, the low concentration of the reacting chemical species at the catalyst surface leads to a first-order kinetics [27].

For first-order kinetics, the local effectiveness factor depends on the value of the dimensionless local Thiele modulus (local is related to the washcoat). The generalized local Thiele modulus can be defined as

$$\phi_{L,i} = \delta_c \sqrt{\frac{k_{V,i}}{D_{\mathrm{eff},i}}} \tag{A.1}$$

The generalized Thiele method uses a generic characteristic length, δ_c, for any geometry as the ratio of catalyst volume to external surface area. Because the thickness of the catalytic layer over the passage hydraulic diameter is very small (25 μm, see Table 2) it can be assumed that the washcoat of the TWC may be viewed as a flat-plate [10], of thickness δ_c (see Fig. 3). Since the washcoat layer can be approximated as an infinite slab, the generic solution for the local effectiveness factor can be approximated by [24]:

$$\eta_{L,i} = \frac{\tanh(\phi_{L,i})}{\phi_{L,i}} \tag{A.2}$$

The above analysis is exact for a chemical specie that dissociates isothermally in the catalytic washcoat, following a first order reaction rate. Zygourakis and Aris [11], using the Prater relation, have observed the validity of the isothermal washcoat assumption. They have concluded that for reactant concentrations encountered in automotive

TWC, the temperature change within the washcoat is less than 1 °C. Using finite-element analysis, Hayes and Kolaczkowski [9] have also concluded that the TWC washcoat can be considered isothermal.

For non linear kinetics and for more non-uniform washcoat shapes it is necessary to compute numerically the local effectiveness factor. In the literature there are available approximation methods for the estimation of local effectiveness factor under such conditions [28].

Appendix B. Evaluation of the effective diffusion in the washcoat

Because the importance of the internal mass transport, it is necessary to have reliable information on the mass transport rate in the porous medium. Inside the porous washcoat, convective transport can be neglected. On the contrary, the diffusive mass transport may have a significant influence on the conversion behavior of the TWC, and thus the evaluation of the effective diffusion coefficients of exhaust gases in the washcoat layer is needed.

Internal diffusion of species into the porous solid that includes macropore, mesopore, and micropore diffusion, depends on the pore diameter. The following nomenclature is common for the description of a porous media:

(a) micropore diffusion or surface diffusion occurs for a pore diameter less than 2 nm and has exponential temperature dependence;
(b) mesopore diffusion occurs for pore diameters $2 < d_p < 50$ nm and is described by Knudsen diffusion through porous solids;
(c) macropore diffusion occurs in large pores typically greater than 50 nm and is described by the same principles as bulk (volume) diffusion.

Recently, various studies [29–32] have used several techniques for obtaining pore-transport characteristics in washcoat layers. Typical sizes of pore diameter in a commercial TWC washcoat range from 6.5 to 500 nm [29], so that micropore diffusion may be neglected.

The washcoat structure can be characterized by the pore diameters d_p, the porosity ε, and the tortuosity factor, τ. The porosity is the ratio of void (open) volume to the total volume of the washcoat including the void volume. The tortuosity factor describes the deviation of the pore geometry from perfect cylindrical shaped pores, and accounts for the tortuous pathways in the structure. Tortuosity, porosity and mean pore diameter were measured experimentally for TWC washcoats by Hayes et al. [29]. The tortuosity factor of the washcoat is 8.1, the porosity 0.41 and the mean pore diameter 10 nm.

The effective diffusivity, $D_{\text{eff},i}$, measures the rate at which a specie i diffuses into a porous medium (here, the washcoat). There are two main theoretical models to define the effective diffusivity: the random pore model and the parallel-pore model. The former was developed by Wakao and Smith [33] and considers a bi-dispersive porous material (material that consists of pores with two distinct pore sizes). The latter was presented by Wheeler [34] for mono-disperse materials (material that consists of pores of one size range only). Hayes et al. [29] have shown that values of $D_{\text{eff},i}$ for the washcoat predicted by the random pore model are approximately seven times larger than those measured. From this, Hayes et al. [29] have concluded that the random pore model is not appropriate for monolith washcoats and have recommended the use of the parallel pore model for an alumina washcoat. According to this model, the porosity and tortuosity of the porous structure can be taken into account by application of the effective diffusion coefficient that leads to:

$$D_{\text{eff},i} = \frac{\varepsilon D_i}{\tau} \tag{B.1}$$

where D_i is a diffusivity that combines the effects of bulk, $D_{\text{b},i}$ (macropore), and Knudsen, $D_{K,i}$ (mesopore), diffusion processes:

$$\frac{1}{D_i} = \frac{1}{D_{\text{b},i}} + \frac{1}{D_{K,i}} \tag{B.2}$$

The temperature dependence of the effective diffusion coefficient differs for volume diffusion and Knudsen diffusion. However, Hayes et al. [29] have concluded that the mesopores were prevalent in the washcoat and therefore the Knudsen diffusion dominates. From this, the effective diffusion coefficient can be written as

$$D_i \approx D_{K,i} = 48.5 d_p \sqrt{\frac{T_W}{10^3 M_i}} \tag{B.3}$$

Eq. (B.3) uses the parallel pore model to represent the porous structure, which is a reasonable model to represent the uni-modal pore size distribution of the TWC washcoat. If one assumes Knudsen diffusion to be dominant, temperature and gas specie dependence of the effective diffusivity can be expressed as

$$D_{\text{eff},i}(T) = D_{\text{eff,ref}} \sqrt{\frac{T_W}{T_{\text{ref}}}} \sqrt{\frac{M_{\text{ref}}}{M_i}} \tag{B.4}$$

where the chosen reference chemical specie is the CO and $T_{\text{ref}} = 296$ K. The agreement between the more recent measured diffusion data [32] and previous experimental results [29,31] is very good. On the other hand, the results predicted by the parallel pore model (Eq. (B.1)) also agree well with the experimental results, and thus when measured data are unavailable, this model is appropriate to predict the effective diffusivity in the TWC washcoat. In the present study, $D_{\text{eff,ref}} = 1.13 \times 10^{-7}\ \text{m}^2\ \text{s}^{-1}$ [32] has been used.

References

[1] V. Tomašić, Z. Gomzi, S. Zrnčević, Analysis and modeling of a monolith reactor, Chem. Eng. Technol. 29 (2006) 59–65.

[2] H. Santos, M. Costa, Analysis of the mass transfer controlled regime in automotive catalytic converters, Int. J. Heat Mass Transfer (2007), doi:10.1016/j.ijheatmasstransfer.2007.04.044.
[3] J. Kašpar, P. Fornasiero, N. Hickey, Automotive catalytic converters: current status and some perspectives, Catal. Today 77 (2003) 419–449.
[4] P. Kočí, F. Štěpánek, M. Kubíček, M. Marek, Meso-scale modeling of CO oxidation in digitally reconstructed porous Pt/γ-Al_2O_3 catalyst, Chem. Eng. Sci. 61 (2006) 3240–3249.
[5] A. Hatton, N. Birkby, J. Hartick, Theoretical and experimental study of mass transfer effects in automotive catalysts, SAE paper 1999-01-3474, 1999.
[6] E. Tronconi, A. Beretta, The role of inter- and intra-phase mass transfer in the SCR–DeNO$_x$ reaction over catalysts of different shapes, Catal. Today 52 (1999) 249–258.
[7] G. Pontikakis, Modeling, reaction schemes and parameter estimation in catalytic converters and diesel filters, Ph.D. Thesis, Mechanical Engineering Department, University of Thessaly, Volos 2003. ⟨http://www.mie.uth.gr/labs/ltte/pubs/PhD_G_Pont.pdf⟩.
[8] G.S. Konstantas, Development and application of a computer aided engineering methodology supporting the design optimization of automotive exhaust treatment systems, Ph.D. Thesis, Mechanical Engineering Department, University of Thessaly, Volos 2006. ⟨http://www.mie.uth.gr/labs/ltte/grk/pubs/PhD_G_Konstantas.pdf⟩.
[9] R.E. Hayes, S.T. Kolaczkowski, Mass and heat transfer effects in catalytic monolith reactors, Chem. Eng. Sci. 49 (1994) 3587–3599.
[10] D. Leung, R.E. Hayes, S.T. Kolaczkowski, Diffusion limitation effects in the washcoat of a catalytic monolith reactor, Canad. J. Chem. Eng. 74 (1996) 94–103.
[11] K. Zygourakis, R. Aris, Multiple oxidation reactions and diffusion in the catalytic layer of monolith reactors, Chem. Eng. Sci. 38 (1983) 733–744.
[12] R.E. Hayes, S.T. Kolaczkowski, P.K.C. Li, S. Awdry, The palladium catalysed oxidation of methane: reaction kinetics and the effect of diffusion barrieres, Chem. Eng. Sci. 56 (2001) 4815–4835.
[13] R.E. Hayes, B. Liu, R. Moxom, M. Votsmeier, The effect of washcoat geometry on mass transfer in monolith reactors, Chem. Eng. Sci. 59 (2004) 3169–3181.
[14] S.H. Chan, D.L. Hoang, Heat transfer and chemical reactions in exhaust system of a cold-start engine, Int. J. Heat Mass Transfer 42 (1999) 4165–4183.
[15] G.C. Koltsakis, P.A. Konstantinidis, A.M. Stamatelos, Development and application range of mathematical models for 3-way catalytic converters, Appl. Catal. B: Environ. 12 (1997) 161–191.
[16] G. Konstantas, A.M. Stamatelos, Modelling three-way catalytic converters: an effort to predict the effect of precious metal loading, Proc. Inst. Mech. Eng. D 221 (2007) 355–373.
[17] N. Baba, K. Ohsawa, S. Sugiura, Numerical approach for improving the conversion characteristics of exhaust catalysts under warming-up condition, SAE paper 962076, 1996.
[18] G. McCullough, R. Douglas, G. Cunnigham, L. Foley, The development of a two-dimensional transient catalyst model for direct injection two-stroke applications, Proc. Inst. Mech. Eng. D 215 (2001) 919–933.
[19] R.D. Hawthorn, Afterburner catalysts-effects of heat and mass transfer between gas and catalyst surface, Amer. Inst. Chem. Eng. 21 (1974) 849–853.
[20] F.P. Incropera, D.P. deWitt, Fundamentals of Heat and Mass Transfer, fourth ed., John Wiley & Sons, 1996.
[21] L. Olsson, B. Andersson, Kinetic modeling in automotive catalysis, Top. Catal. 28 (2004) 89–98.
[22] V. Balakotaiah, D.H. West, Shape normalization and analysis of the mass transfer controlled regime in catalytic monoliths, Chem. Eng. Sci. 57 (2002) 1269–1286.
[23] H.J. Kwon, J.H. Baik, Y.T. Kwon, I.S. Nam, Se H. Oh, Detailed reaction kinetics over commercial three-way catalysts, Chem. Eng. Sci. (2007), doi:10.1016/j.ces.2007.01.082.
[24] R. Aris, The mathematical theory of diffusion and reaction in permeable catalysts, The Theory of the Steady State, vol. 1, Clarendon Press, Oxford, 1975.
[25] L.K. Doory, Development of catalytic reactor designs for enhanced CO oxidation, Ph.D. Thesis, University College, London, 1992.
[26] D. Papadias, L. Edsberg, P. Björnbom, Simplified method for effectiveness factor calculations in irregular geometries of washcoats, Chem. Eng. Sci. 55 (2000) 1447–1459.
[27] C. Dubien, D. Schweich, G. Mabilon, B. Martin, M. Prigent, Three-way catalytic converter modelling: fast- and slow-oxidizing hydrocarbons, inhibiting species, and steam-reforming reaction, Chem. Eng. Sci. 53 (1998) 471–481.
[28] R.E. Hayes, P.K. Mok, J. Mmbaga, M. Votsmeier, A fast approximation method for computing effectiveness factors with non-uniform kinetics, Chem. Eng. Sci. 62 (2007) 2209–2215.
[29] R.E. Hayes, S.T. Kolaczkowski, P.K.C. Li, S. Awdry, Evaluating the effective diffusivity of methane in the washcoat of a honeycomb monolith, Appl. Catal. B: Environ. 25 (2000) 93–104.
[30] S.T. Kolaczkowski, Measurement of effective diffusivity in catalyst-coated monoliths, Catal. Today 83 (2003) 85–95.
[31] F. Zhang, R.E. Hayes, S.T. Kolaczkowski, A new technique to measure the effective diffusivity in the washcoat of a monolith reactor, Chem. Eng. Res. Des. 82 (A4) (2004) 481–489.
[32] T. Starý, O. Šolcová, P. Schneider, M. Marek, Effective diffusivities and pore-transport characteristics of washcoated ceramic monolith for automotive catalytic converter, Chem. Eng. Sci. 61 (2006) 5934–5943.
[33] N. Wakao, J.M. Smith, Diffusion in catalyst pellets, Chem. Eng. Sci. 17 (1962) 825–834.
[34] A. Wheeler, in: P.H. Emmett (Ed.), Catalysis, vol. II, Reinhold, New York, 1955, p. 105, Chapter 2.